PHYSICAL REVIEW D **82,** 011502(R) (2010)

B-meson decays to $\eta'\rho$, $\eta' f_0$, and $\eta' K^*$

P. del Amo Sanchez,[1] J. P. Lees,[1] V. Poireau,[1] E. Prencipe,[1] V. Tisserand,[1] J. Garra Tico,[2] E. Grauges,[2] M. Martinelli,[3a,3b] A. Palano,[3a,3b] M. Pappagallo,[3a,3b] G. Eigen,[4] B. Stugu,[4] L. Sun,[4] M. Battaglia,[5] D. N. Brown,[5] B. Hooberman,[5] L. T. Kerth,[5] Yu. G. Kolomensky,[5] G. Lynch,[5] I. L. Osipenkov,[5] T. Tanabe,[5] C. M. Hawkes,[6] A. T. Watson,[6] H. Koch,[7] T. Schroeder,[7] D. J. Asgeirsson,[8] C. Hearty,[8] T. S. Mattison,[8] J. A. McKenna,[8] A. Khan,[9] A. Randle-Conde,[9] V. E. Blinov,[10] A. R. Buzykaev,[10] V. P. Druzhinin,[10] V. B. Golubev,[10] A. P. Onuchin,[10] S. I. Serednyakov,[10] Yu. I. Skovpen,[10] E. P. Solodov,[10] K. Yu. Todyshev,[10] A. N. Yushkov,[10] M. Bondioli,[11] S. Curry,[11] D. Kirkby,[11] A. J. Lankford,[11] M. Mandelkern,[11] E. C. Martin,[11] D. P. Stoker,[11] H. Atmacan,[12] J. W. Gary,[12] F. Liu,[12] O. Long,[12] G. M. Vitug,[12] C. Campagnari,[13] T. M. Hong,[13] D. Kovalskyi,[13] J. D. Richman,[13] A. M. Eisner,[14] C. A. Heusch,[14] J. Kroseberg,[14] W. S. Lockman,[14] A. J. Martinez,[14] T. Schalk,[14] B. A. Schumm,[14] A. Seiden,[14] L. O. Winstrom,[14] C. H. Cheng,[15] D. A. Doll,[15] B. Echenard,[15] D. G. Hitlin,[15] P. Ongmongkolkul,[15] F. C. Porter,[15] A. Y. Rakitin,[15] R. Andreassen,[16] M. S. Dubrovin,[16] G. Mancinelli,[16] B. T. Meadows,[16] M. D. Sokoloff,[16] P. C. Bloom,[17] W. T. Ford,[17] A. Gaz,[17] J. F. Hirschauer,[17] M. Nagel,[17] U. Nauenberg,[17] A. Penzkofer,[17] J. G. Smith,[17] S. R. Wagner,[17] R. Ayad,[18,*] W. H. Toki,[18] T. M. Karbach,[19] J. Merkel,[19] A. Petzold,[19] B. Spaan,[19] K. Wacker,[19] M. J. Kobel,[20] K. R. Schubert,[20] R. Schwierz,[20] D. Bernard,[21] M. Verderi,[21] P. J. Clark,[22] S. Playfer,[22] J. E. Watson,[22] M. Andreotti,[23a,23b] D. Bettoni,[23a] C. Bozzi,[23a] R. Calabrese,[23a,23b] A. Cecchi,[23a,23b] G. Cibinetto,[23a,23b] E. Fioravanti,[23a,23b] P. Franchini,[23a,23b] E. Luppi,[23a,23b] M. Munerato,[23a,23b] M. Negrini,[23a,23b] A. Petrella,[23a,23b] L. Piemontese,[23a] R. Baldini-Ferroli,[24] A. Calcaterra,[24] R. de Sangro,[24] G. Finocchiaro,[24] M. Nicolaci,[24] S. Pacetti,[24] P. Patteri,[24] I. M. Peruzzi,[24,†] M. Piccolo,[24] M. Rama,[24] A. Zallo,[24] R. Contri,[25a,25b] E. Guido,[25a,25b] M. Lo Vetere,[25a,25b] M. R. Monge,[25a,25b] S. Passaggio,[25a] C. Patrignani,[25a,25b] E. Robutti,[25a] S. Tosi,[25a,25b] B. Bhuyan,[26] C. L. Lee,[27] M. Morii,[27] A. Adametz,[28] J. Marks,[28] S. Schenk,[28] U. Uwer,[28] F. U. Bernlochner,[29] H. M. Lacker,[29] T. Lueck,[29] A. Volk,[29] P. D. Dauncey,[30] M. Tibbetts,[30] P. K. Behera,[31] U. Mallik,[31] C. Chen,[32] J. Cochran,[32] H. B. Crawley,[32] L. Dong,[32] W. T. Meyer,[32] S. Prell,[32] E. I. Rosenberg,[32] A. E. Rubin,[32] Y. Y. Gao,[33] A. V. Gritsan,[33] Z. J. Guo,[33] N. Arnaud,[34] M. Davier,[34] D. Derkach,[34] J. Firmino da Costa,[34] G. Grosdidier,[34] F. Le Diberder,[34] A. M. Lutz,[34] B. Malaescu,[34] A. Perez,[34] P. Roudeau,[34] M. H. Schune,[34] J. Serrano,[34] V. Sordini,[34,‡] A. Stocchi,[34] L. Wang,[34] G. Wormser,[34] D. J. Lange,[35] D. M. Wright,[35] I. Bingham,[36] J. P. Burke,[36] C. A. Chavez,[36] J. P. Coleman,[36] J. R. Fry,[36] E. Gabathuler,[36] R. Gamet,[36] D. E. Hutchcroft,[36] D. J. Payne,[36] C. Touramanis,[36] A. J. Bevan,[37] F. Di Lodovico,[37] R. Sacco,[37] M. Sigamani,[37] G. Cowan,[38] S. Paramesvaran,[38] A. C. Wren,[38] D. N. Brown,[39] C. L. Davis,[39] A. G. Denig,[40] M. Fritsch,[40] W. Gradl,[40] A. Hafner,[40] K. E. Alwyn,[41] D. Bailey,[41] R. J. Barlow,[41] G. Jackson,[41] G. D. Lafferty,[41] T. J. West,[41] J. Anderson,[42] R. Cenci,[42] A. Jawahery,[42] D. A. Roberts,[42] G. Simi,[42] J. M. Tuggle,[42] C. Dallapiccola,[43] E. Salvati,[43] R. Cowan,[44] D. Dujmic,[44] P. H. Fisher,[44] G. Sciolla,[44] M. Zhao,[44] D. Lindemann,[45] P. M. Patel,[45] S. H. Robertson,[45] M. Schram,[45] P. Biassoni,[46a,46b] A. Lazzaro,[46a,46b] V. Lombardo,[46a] F. Palombo,[46a,46b] S. Stracka,[46a,46b] F. C. Ungaro,[46a] L. Cremaldi,[47] R. Godang,[47,§] R. Kroeger,[47] P. Sonnek,[47] D. J. Summers,[47] H. W. Zhao,[47] X. Nguyen,[48] M. Simard,[48] P. Taras,[48] G. De Nardo,[49a,49b] D. Monorchio,[49a,49b] G. Onorato,[49a,49b] C. Sciacca,[49a,49b] G. Raven,[50] H. L. Snoek,[50] C. P. Jessop,[51] K. J. Knoepfel,[51] J. M. LoSecco,[51] W. F. Wang,[51] L. A. Corwin,[52] K. Honscheid,[52] R. Kass,[52] J. P. Morris,[52] A. M. Rahimi,[52] N. L. Blount,[53] J. Brau,[53] R. Frey,[53] O. Igonkina,[53] J. A. Kolb,[53] R. Rahmat,[53] N. B. Sinev,[53] D. Strom,[53] J. Strube,[53] E. Torrence,[53] G. Castelli,[54a,54b] E. Feltresi,[54a,54b] N. Gagliardi,[54a,54b] M. Margoni,[54a,54b] M. Morandin,[54a] M. Posocco,[54a] M. Rotondo,[54a] F. Simonetto,[54a,54b] R. Stroili,[54a,54b] E. Ben-Haim,[55] G. R. Bonneaud,[55] H. Briand,[55] G. Calderini,[55] J. Chauveau,[55] O. Hamon,[55] Ph. Leruste,[55] G. Marchiori,[55] J. Ocariz,[55] J. Prendki,[55] S. Sitt,[55] M. Biasini,[56a,56b] E. Manoni,[56a,56b] C. Angelini,[57a,57b] G. Batignani,[57a,57b] S. Bettarini,[57a,57b] M. Carpinelli,[57a,57b,‖] G. Casarosa,[57a,57b] A. Cervelli,[57a,57b] F. Forti,[57a,57b] M. A. Giorgi,[57a,57b] A. Lusiani,[57c] N. Neri,[57a,57b] E. Paoloni,[57a,57b] G. Rizzo,[57a,57b] J. J. Walsh,[57a] D. Lopes Pegna,[58] C. Lu,[58] J. Olsen,[58] A. J. S. Smith,[58] A. V. Telnov,[58] F. Anulli,[59a] E. Baracchini,[59a,59b] G. Cavoto,[59a] R. Faccini,[59a,59b] F. Ferrarotto,[59a] F. Ferroni,[59a,59b] M. Gaspero,[59a,59b] L. Li Gioi,[59a] M. A. Mazzoni,[59a] G. Piredda,[59a] F. Renga,[59a,59b] M. Ebert,[60] T. Hartmann,[60] T. Leddig,[60] H. Schröder,[60] R. Waldi,[60] T. Adye,[61] B. Franek,[61] E. O. Olaiya,[61] F. F. Wilson,[61] S. Emery,[62] G. Hamel de Monchenault,[62] G. Vasseur,[62] Ch. Yèche,[62] M. Zito,[62] M. T. Allen,[63] D. Aston,[63] D. J. Bard,[63] R. Bartoldus,[63] J. F. Benitez,[63] C. Cartaro,[63] M. R. Convery,[63] J. Dorfan,[63] G. P. Dubois-Felsmann,[63] W. Dunwoodie,[63] R. C. Field,[63] M. Franco Sevilla,[63] B. G. Fulsom,[63] A. M. Gabareen,[63] M. T. Graham,[63] P. Grenier,[63] C. Hast,[63] W. R. Innes,[63] M. H. Kelsey,[63] H. Kim,[63] P. Kim,[63] M. L. Kocian,[63] D. W. G. S. Leith,[63] S. Li,[63] B. Lindquist,[63] S. Luitz,[63] V. Luth,[63] H. L. Lynch,[63] D. B. MacFarlane,[63] H. Marsiske,[63] D. R. Muller,[63] H. Neal,[63] S. Nelson,[63] C. P. O'Grady,[63] I. Ofte,[63] M. Perl,[63] T. Pulliam,[63] B. N. Ratcliff,[63] A. Roodman,[63] A. A. Salnikov,[63] V. Santoro,[63] R. H. Schindler,[63] J. Schwiening,[63]

A. Snyder,[63] D. Su,[63] M. K. Sullivan,[63] S. Sun,[63] K. Suzuki,[63] J. M. Thompson,[63] J. Va'vra,[63] A. P. Wagner,[63] M. Weaver,[63] C. A. West,[63] W. J. Wisniewski,[63] M. Wittgen,[63] D. H. Wright,[63] H. W. Wulsin,[63] A. K. Yarritu,[63] C. C. Young,[63] V. Ziegler,[63] X. R. Chen,[64] W. Park,[64] M. V. Purohit,[64] R. M. White,[64] J. R. Wilson,[64] S. J. Sekula,[65] M. Bellis,[66] P. R. Burchat,[66] A. J. Edwards,[66] T. S. Miyashita,[66] S. Ahmed,[67] M. S. Alam,[67] J. A. Ernst,[67] B. Pan,[67] M. A. Saeed,[67] S. B. Zain,[67] N. Guttman,[68] A. Soffer,[68] P. Lund,[69] S. M. Spanier,[69] R. Eckmann,[70] J. L. Ritchie,[70] A. M. Ruland,[70] C. J. Schilling,[70] R. F. Schwitters,[70] B. C. Wray,[70] J. M. Izen,[71] X. C. Lou,[71] F. Bianchi,[72a,72b] D. Gamba,[72a,72b] M. Pelliccioni,[72a,72b] M. Bomben,[73a,73b] L. Lanceri,[73a,73b] L. Vitale,[73a,73b] N. Lopez-March,[74] F. Martinez-Vidal,[74] D. A. Milanes,[74] A. Oyanguren,[74] J. Albert,[75] Sw. Banerjee,[75] H. H. F. Choi,[75] K. Hamano,[75] G. J. King,[75] R. Kowalewski,[75] M. J. Lewczuk,[75] I. M. Nugent,[75] J. M. Roney,[75] R. J. Sobie,[75] T. J. Gershon,[76] P. F. Harrison,[76] J. Ilic,[76] T. E. Latham,[76] E. M. T. Puccio,[76] H. R. Band,[77] X. Chen,[77] S. Dasu,[77] K. T. Flood,[77] Y. Pan,[77] R. Prepost,[77] C. O. Vuosalo,[77] and S. L. Wu[77]

[1]*Laboratoire d'Annecy-le-Vieux de Physique des Particules (LAPP), Université de Savoie, CNRS/IN2P3, F-74941 Annecy-Le-Vieux, France*
[2]*Universitat de Barcelona, Facultat de Fisica, Departament ECM, E-08028 Barcelona, Spain*
[3a]*INFN Sezione di Bari, I-70126 Bari, Italy*
[3b]*Dipartimento di Fisica, Università di Bari, I-70126 Bari, Italy*
[4]*University of Bergen, Institute of Physics, N-5007 Bergen, Norway*
[5]*Lawrence Berkeley National Laboratory and University of California, Berkeley, California 94720, USA*
[6]*University of Birmingham, Birmingham, B15 2TT, United Kingdom*
[7]*Ruhr Universität Bochum, Institut für Experimentalphysik 1, D-44780 Bochum, Germany*
[8]*University of British Columbia, Vancouver, British Columbia, Canada V6T 1Z1*
[9]*Brunel University, Uxbridge, Middlesex UB8 3PH, United Kingdom*
[10]*Budker Institute of Nuclear Physics, Novosibirsk 630090, Russia*
[11]*University of California at Irvine, Irvine, California 92697, USA*
[12]*University of California at Riverside, Riverside, California 92521, USA*
[13]*University of California at Santa Barbara, Santa Barbara, California 93106, USA*
[14]*University of California at Santa Cruz, Institute for Particle Physics, Santa Cruz, California 95064, USA*
[15]*California Institute of Technology, Pasadena, California 91125, USA*
[16]*University of Cincinnati, Cincinnati, Ohio 45221, USA*
[17]*University of Colorado, Boulder, Colorado 80309, USA*
[18]*Colorado State University, Fort Collins, Colorado 80523, USA*
[19]*Technische Universität Dortmund, Fakultät Physik, D-44221 Dortmund, Germany*
[20]*Technische Universität Dresden, Institut für Kern- und Teilchenphysik, D-01062 Dresden, Germany*
[21]*Laboratoire Leprince-Ringuet, CNRS/IN2P3, Ecole Polytechnique, F-91128 Palaiseau, France*
[22]*University of Edinburgh, Edinburgh EH9 3JZ, United Kingdom*
[23a]*INFN Sezione di Ferrara, I-44100 Ferrara, Italy*
[23b]*Dipartimento di Fisica, Università di Ferrara, I-44100 Ferrara, Italy*
[24]*INFN Laboratori Nazionali di Frascati, I-00044 Frascati, Italy*
[25a]*INFN Sezione di Genova, I-16146 Genova, Italy*
[25b]*Dipartimento di Fisica, Università di Genova, I-16146 Genova, Italy*
[26]*Indian Institute of Technology Guwahati, Guwahati, Assam, 781 039, India*
[27]*Harvard University, Cambridge, Massachusetts 02138, USA*
[28]*Universität Heidelberg, Physikalisches Institut, Philosophenweg 12, D-69120 Heidelberg, Germany*
[29]*Humboldt-Universität zu Berlin, Institut für Physik, Newtonstr. 15, D-12489 Berlin, Germany*
[30]*Imperial College London, London, SW7 2AZ, United Kingdom*
[31]*University of Iowa, Iowa City, Iowa 52242, USA*
[32]*Iowa State University, Ames, Iowa 50011-3160, USA*
[33]*Johns Hopkins University, Baltimore, Maryland 21218, USA*
[34]*Laboratoire de l'Accélérateur Linéaire, IN2P3/CNRS et Université Paris-Sud 11, Centre Scientifique d'Orsay, B. P. 34, F-91898 Orsay Cedex, France*
[35]*Lawrence Livermore National Laboratory, Livermore, California 94550, USA*
[36]*University of Liverpool, Liverpool L69 7ZE, United Kingdom*
[37]*Queen Mary, University of London, London, E1 4NS, United Kingdom*
[38]*University of London, Royal Holloway and Bedford New College, Egham, Surrey TW20 0EX, United Kingdom*
[39]*University of Louisville, Louisville, Kentucky 40292, USA*
[40]*Johannes Gutenberg-Universität Mainz, Institut für Kernphysik, D-55099 Mainz, Germany*
[41]*University of Manchester, Manchester M13 9PL, United Kingdom*
[42]*University of Maryland, College Park, Maryland 20742, USA*

[43]*University of Massachusetts, Amherst, Massachusetts 01003, USA*
[44]*Massachusetts Institute of Technology, Laboratory for Nuclear Science, Cambridge, Massachusetts 02139, USA*
[45]*McGill University, Montréal, Québec, Canada H3A 2T8*
[46a]*INFN Sezione di Milano, I-20133 Milano, Italy*
[46b]*Dipartimento di Fisica, Università di Milano, I-20133 Milano, Italy*
[47]*University of Mississippi, University, Mississippi 38677, USA*
[48]*Université de Montréal, Physique des Particules, Montréal, Québec, Canada H3C 3J7*
[49a]*INFN Sezione di Napoli, I-80126 Napoli, Italy*
[49b]*Dipartimento di Scienze Fisiche, Università di Napoli Federico II, I-80126 Napoli, Italy*
[50]*NIKHEF, National Institute for Nuclear Physics and High Energy Physics, NL-1009 DB Amsterdam, The Netherlands*
[51]*University of Notre Dame, Notre Dame, Indiana 46556, USA*
[52]*Ohio State University, Columbus, Ohio 43210, USA*
[53]*University of Oregon, Eugene, Oregon 97403, USA*
[54a]*INFN Sezione di Padova, I-35131 Padova, Italy*
[54b]*Dipartimento di Fisica, Università di Padova, I-35131 Padova, Italy*
[55]*Laboratoire de Physique Nucléaire et de Hautes Energies, IN2P3/CNRS, Université Pierre et Marie Curie-Paris6, Université Denis Diderot-Paris7, F-75252 Paris, France*
[56a]*INFN Sezione di Perugia, I-06100 Perugia, Italy*
[56b]*Dipartimento di Fisica, Università di Perugia, I-06100 Perugia, Italy*
[57a]*INFN Sezione di Pisa, I-56127 Pisa, Italy*
[57b]*Dipartimento di Fisica, Università di Pisa, I-56127 Pisa, Italy*
[57c]*Scuola Normale Superiore di Pisa, I-56127 Pisa, Italy*
[58]*Princeton University, Princeton, New Jersey 08544, USA*
[59a]*INFN Sezione di Roma, I-00185 Roma, Italy*
[59b]*Dipartimento di Fisica, Università di Roma La Sapienza, I-00185 Roma, Italy*
[60]*Universität Rostock, D-18051 Rostock, Germany*
[61]*Rutherford Appleton Laboratory, Chilton, Didcot, Oxon, OX11 0QX, United Kingdom*
[62]*CEA, Irfu, SPP, Centre de Saclay, F-91191 Gif-sur-Yvette, France*
[63]*SLAC National Accelerator Laboratory, Stanford, California 94309 USA*
[64]*University of South Carolina, Columbia, South Carolina 29208, USA*
[65]*Southern Methodist University, Dallas, Texas 75275, USA*
[66]*Stanford University, Stanford, California 94305-4060, USA*
[67]*State University of New York, Albany, New York 12222, USA*
[68]*Tel Aviv University, School of Physics and Astronomy, Tel Aviv, 69978, Israel*
[69]*University of Tennessee, Knoxville, Tennessee 37996, USA*
[70]*University of Texas at Austin, Austin, Texas 78712, USA*
[71]*University of Texas at Dallas, Richardson, Texas 75083, USA*
[72a]*INFN Sezione di Torino, I-10125 Torino, Italy*
[72b]*Dipartimento di Fisica Sperimentale, Università di Torino, I-10125 Torino, Italy*
[73a]*INFN Sezione di Trieste, I-34127 Trieste, Italy*
[73b]*Dipartimento di Fisica, Università di Trieste, I-34127 Trieste, Italy*
[74]*IFIC, Universitat de Valencia-CSIC, E-46071 Valencia, Spain*
[75]*University of Victoria, Victoria, British Columbia, Canada V8W 3P6*
[76]*Department of Physics, University of Warwick, Coventry CV4 7AL, United Kingdom*
[77]*University of Wisconsin, Madison, Wisconsin 53706, USA*
(Received 5 April 2010; published 29 July 2010)

We present measurements of *B*-meson decays to the final states $\eta'\rho$, $\eta' f_0$, and $\eta' K^*$, where K^* stands for a vector, scalar, or tensor strange meson. We observe a significant signal or evidence for $\eta'\rho^+$ and all the $\eta' K^*$ channels. We also measure, where applicable, the charge asymmetries, finding results consistent with no direct *CP* violation in all cases. The measurements are performed on a data sample consisting of 467×10^6 $B\bar{B}$ pairs, collected with the *BABAR* detector at the PEP-II e^+e^- collider at the SLAC National Accelerator Laboratory. Our results favor the theoretical predictions from perturbative QCD and QCD

[*]Present address: Temple University, Philadelphia, PA 19122, USA.
[†]Also at Università di Perugia, Dipartimento di Fisica, Perugia, Italy.
[‡]Also at Università di Roma La Sapienza, I-00185 Roma, Italy.
[§]Present address: University of South Alabama, Mobile, AL 36688, USA.
[‖]Also at Università di Sassari, Sassari, Italy.

factorization and we observe an enhancement of the tensor $K_2^*(1430)$ with respect to the vector $K^*(892)$ component.

DOI: 10.1103/PhysRevD.82.011502 PACS numbers: 13.25.Hw, 12.15.Hh, 11.30.Er

Charmless two-body decays of B mesons are a powerful probe for testing the standard model and searching for new physics phenomena [1]. Decays to final states containing η or η' mesons exhibit a distinctive pattern of interference among the dominant amplitudes and are also sensitive to a potentially large flavor-singlet contribution [2]. B meson decays to the final states $\eta'\rho$ and $\eta' K^*(892)$ have been investigated theoretically within the standard model by means of perturbative QCD (pQCD) [3], QCD factorization (QCDF) [4], soft collinear effective theory (SCET) [5], and $SU(3)$ flavor symmetry [6]. The predicted branching fractions to the final states $\eta' K^*(892)^+$ and $\eta' K^*(892)^0$ are in the range of a few times 10^{-6}, whereas the branching fraction for $B^0 \to \eta'\rho^0$ is suppressed to $10^{-7} - 10^{-8}$. There is some disagreement on the predictions of the branching fraction for $B^+ \to \eta'\rho^+$: SCET calculations give a value of 0.4×10^{-6}, whereas pQCD and QCDF predict a branching fraction of $(6\text{–}9) \times 10^{-6}$. There are no theoretical predictions for the branching fraction of $B^0 \to \eta' f_0$.

Experimentally, searches for these decays have been performed by the *BABAR* [7] and Belle [8] collaborations. The former claimed evidence for the $\eta'\rho^+$, $\eta' K^*(892)^+$, and $\eta' K^*(892)^0$ final states, while the latter establishes upper limits that are in poor agreement with the branching fractions, in the range $(4\text{–}9) \times 10^{-6}$, measured by *BABAR*.

Very few predictions exist for B-meson decays to $\eta' K_0^*(1430)$ and $\eta' K_2^*(1430)$. In Ref. [9], based on pQCD, the branching fraction of $B \to \eta' K_0^*(1430)$ is predicted to be in the range $(20\text{–}80) \times 10^{-6}$, while in Ref. [10] the branching fraction of $B \to \eta' K_2^*(1430)$ is calculated to be $\sim 2 \times 10^{-6}$, exploiting QCDF calculations. No searches for the $\eta' K_0^*(1430)$ and $\eta' K_2^*(1430)$ final states have been reported. In a recent study of $B \to \omega K^*$ decays [11], where K^* denotes the spin 0, 1, or 2 states $K_0^*(1430)$, $K^*(892)$, and $K_2^*(1430)$, the tensor and scalar K^* components were found to be significantly larger than the vector $K^*(892)$, a fact which was not anticipated by theory.

In this paper, we report measurements of the branching fractions of B mesons decaying to the final states $\eta'\rho$, $\eta' f_0$, and $\eta' K^*$. Where applicable, we also measure the charge asymmetry $\mathcal{A}_{\rm ch} \equiv (\Gamma^- - \Gamma^+)/(\Gamma^- + \Gamma^+)$, where the superscript to the decay width Γ refers to the charge of the $B^\pm$ meson or to the charge of the kaon in the neutral B decays.

For this analysis, we use the full *BABAR* dataset, collected at the PEP-II asymmetric-energy e^+e^- collider located at the SLAC National Accelerator Laboratory, consisting of 467×10^6 $B\bar{B}$ pairs originating from the decay of the $\Upsilon(4S)$ resonance, produced at a center-of-mass energy $\sqrt{s} = 10.58$ GeV. The *BABAR* detector is described in detail elsewhere [12].

We reconstruct B-daughter candidates through their decays $\eta' \to \eta\pi^+\pi^-$ $(\eta'_{\eta\pi\pi})$, $\eta' \to \rho^0\gamma$ $(\eta'_{\rho\gamma})$, $\eta \to \gamma\gamma$, $\rho^+ \to \pi^+\pi^0$, $\rho^0 \to \pi^+\pi^-$, $f_0(980) \to \pi^+\pi^-$ [13], $K^{*0} \to K^+\pi^-$, $K^{*+} \to K^+\pi^0$ $(K^{*+}_{K^+\pi^0})$, $K^{*+} \to K^0_S\pi^+$ $(K^{*+}_{K^0_S\pi^+})$, $K^0_S \to \pi^+\pi^-$, and $\pi^0 \to \gamma\gamma$. We use both $\eta' \to \eta\pi^+\pi^-$ and $\eta' \to \rho^0\gamma$ for $\eta' K^*$, but due to the larger backgrounds affecting the $\eta'_{\rho\gamma}$ channel, we do not use the $\eta' \to \rho^0\gamma$ decay mode for the $\eta'\rho$ and $\eta' f_0$ final states. We require the invariant masses of the B-daughter candidates to satisfy the following requirements: $910 < m(\eta') < 1000$ MeV, $510 < m(\eta) < 580$ MeV, $510 < m(\rho/f_0) < 1060$ MeV, $750 < m(K^*) < 1550$ MeV, $488 < m(K^0_S) < 508$ MeV, and $120 < m(\pi^0) < 150$ MeV; these mass intervals are chosen to include sidebands to estimate the background levels. We require the photon energy of the π^0 candidates to be greater than 30 MeV in the laboratory frame, while the minimum energy is 100 MeV for the photons of η candidates and 200 MeV for the photons from the $\eta' \to \rho^0\gamma$ decay. A fit constraining the two pion tracks from the K^0_S decay to originate from the same decay vertex is performed and a K^0_S candidate is selected if its flight length exceeds 3 times its uncertainty. Daughter particles from η', η, ρ, f_0, and K^* decays are rejected if their particle identification signatures are consistent with those of electrons or protons; K^+ candidates are required to be positively identified as kaons, and pions must fail this criterion. Unless otherwise stated, charge-conjugate reactions are always implied.

A B-meson candidate is characterized by two kinematic variables, whose small correlation is accounted for in the correction of the fit bias: the energy substituted mass $\mathrm{m_{ES}} \equiv \sqrt{s/4 - \mathbf{p}_B^2}$ and the energy difference $\Delta E \equiv E_B - \sqrt{s}/2$, where $(E_B, \mathbf{p}_B)$ is the B-meson four-momentum vector in the $\Upsilon(4S)$ rest frame. Signal events peak at 0 in ΔE and at the B mass [14] in $m_{\rm ES}$, with a resolution in ΔE ($m_{\rm ES}$) of 20–35 MeV (3 MeV). We select events with $5.25 < \mathrm{m_{ES}} < 5.29$ GeV and $|\Delta E| < 0.2$ GeV.

The dominant backgrounds arise from random combinations of particles in continuum $e^+e^- \to q\bar{q}$ events ($q = u, d, s, c$). The angle θ_T between the thrust axis [15] of the B candidate in the $\Upsilon(4S)$ rest frame and that of the remaining particles in the event is used to suppress this background. Jet-like continuum events peak at $|\cos\theta_T|$ close to 1, while spherical B decays exhibit a flat distribution for this variable. Further rejection is achieved by restricting the range of the helicity angle of the ρ or K^* meson. The helicity angle $\theta_{\mathcal{H}}$ is defined in the rest frame of the ρ or K^* and corresponds to the angle between two vectors: one is the momentum of the daughter pion and the other is the

direction of the boost into this rest frame from the B meson rest frame; for the ρ^+ candidate, we use the positively charged pion. Table I summarizes the requirements we apply on $|\cos\theta_T|$ and $\cos\theta_{\mathcal{H}}$. After the selection criteria have been applied, the average number of combinations per event in data is between 1.1 and 1.3, and we select the candidate with the highest χ^2 probability in a geometric fit to a common B-decay vertex. In this way the probability of selecting the correctly reconstructed event is a few percent higher with respect to a random selection.

Further signal/background separation is provided by a Fisher discriminant $\mathcal{F}$ exploiting four variables sensitive to the production dynamics and event shape: the polar angles, with respect to the beam axis in the e^+e^- center-of-mass frame, of the B candidate momentum and of the B thrust axis; and the zeroth and second angular moments $L_{0,2}$ of the energy flow, excluding the B candidate. The moments are defined by $L_j = \sum_i p_i \times |\cos\theta_i|^j$, where i labels a track or neutral cluster, θ_i is its angle with respect to the B thrust axis, and p_i is its momentum. The mean of $\mathcal{F}$ is shifted so that it is independent of the B-flavor tagging category [16] for $q\bar{q}$ background. The Fisher variable provides about 1 standard deviation discrimination between B-decay events and continuum background.

We obtain the yields and the charge asymmetries $\mathcal{A}_{\rm ch}$ from extended maximum-likelihood fits to the six observables: ΔE, $m_{\rm ES}$, $\mathcal{F}$, the masses of the two resonance candidates $m_{\eta'}$ and $m_{\rho/f_0/K^*}$, and $\cos\theta_{\mathcal{H}}$. The fits distinguish among several categories: $q\bar{q}$ background, $B\bar{B}$ background, and signal component(s) (one for $\eta'\rho^+$, two for $\eta'\rho^0/f_0$, and three for the $\eta' K^*$ modes). For each event i and category j, we define the probability density functions (PDFs) $\mathcal{P}_j(x)$ for the variable x, with the resulting likelihood $\mathcal{L}$:

$$\mathcal{P}^i_j = \mathcal{P}_j(\mathrm{m}^i_{\rm ES})\mathcal{P}_j(\Delta E^i)\mathcal{P}_j(\mathcal{F}^i) \tag{1}$$

$$\mathcal{P}_j(m^i_{\eta'})\mathcal{P}_j(m^i_{\rho/f_0/K^*})\mathcal{P}_j(\cos\theta^i_{\mathcal{H}}),$$
$$\mathcal{L} = \frac{e^{-\sum_j Y_j}}{N!}\prod_{i=1}^{N}\sum_j Y_j\mathcal{P}^i_j, \tag{2}$$

TABLE I. Selection requirements on $\cos\theta_T$ and $\cos\theta_{\mathcal{H}}$ for the different modes.

State	$\lvert\cos\theta_T\rvert$	$\cos\theta_{\mathcal{H}}$ range
$\eta'\rho^0/f_0$	<0.9	$[-0.95, 0.95]$
$\eta'\rho^+$	<0.9	$[-0.80, 1]$
$\eta'_{\eta\pi\pi}K^{*0}$	<0.9	$[-0.85, 1]$
$\eta'_{\rho\gamma}K^{*0}$	<0.6	$[-0.85, 1]$
$\eta'_{\eta\pi\pi}K^{*+}_{K^+\pi^0}$	<0.9	$[-0.75, 1]$
$\eta'_{\rho\gamma}K^{*+}_{K^+\pi^0}$	<0.7	$[-0.75, 1]$
$\eta'_{\eta\pi\pi}K^{*+}_{K^+\pi^0}$	<0.9	$[-0.90, 1]$
$\eta'_{\rho\gamma}K^{*+}_{K^+\pi^0}$	<0.7	$[-0.90, 1]$

where Y_j is the yield for category j, and N is the number of events entering the fit. Where applicable, we split the yields by the flavor of the decaying B meson in order to measure $\mathcal{A}_{\rm ch}$. We find correlations among the observables to be significant in the $B\bar{B}$ components, whereas those are small in the data samples, which contain mostly $q\bar{q}$ background. An exception occurs in the $B^+ \to \eta'_{\rho\gamma}K^{*+}_{K^+\pi^0}$ mode, for which the correlation between m_{K^*} and $\cos\theta_{\mathcal{H}}$, if not taken into account, may cause large biases in the yield of the different K^* components. In this case the factors for $m^i_{K^*}$ and $\cos\theta^i_{\mathcal{H}}$ in Eq. (1) are replaced with a two-dimensional nonparametric PDF [17]. We discuss below our treatment of the somewhat larger correlations found in simulated signal events.

The signal component is studied from the Monte Carlo (MC) simulation [18] of the decay process and the response of the detector and reconstruction chain. Signal events selected in simulation contain both properly reconstructed and incorrectly reconstructed B-meson candidates, which are labeled as ''self-crossfeed'' (SXF). SXF occurs either when some particles from the correct parent B meson are incorrectly assigned to intermediate resonances or when particles from the rest of the event are used in the signal B reconstruction. The fraction of SXF events ranges between 14% and 32% and we do not separate correctly reconstructed events from SXF in the fit. For the scalar $K\pi$ component, we use the LASS model [19,20], which consists of the $K^*_0(1430)$ resonance together with an effective-range nonresonant component. Backgrounds arising from $B\bar{B}$ decays to charmless final states are modeled from the simulation. We select the channels (20–40 for each final state) which have a high probability of passing our selection and build a sample of simulated specimens of these, weighting each component by its branching fraction, either measured or estimated. We model from this sample the PDFs for the $B\bar{B}$ background component and fix its yield (25–350 events, depending on the final state) to the MC prediction. Backgrounds arising from $b \to c$ transitions have distributions very similar to those of $q\bar{q}$ events and thus they are absorbed by the continuum component. For the $\eta'\rho$ modes, we estimate the contribution of the nonresonant $\eta'\pi\pi$ with a fit of the data, selecting only the central region (which excludes the region across the ρ and f_0 resonances) of the $\eta'\pi\pi$ Dalitz plot. The expected nonresonant component is then included in the charmless $B\bar{B}$ background PDF. This procedure is not necessary for the $\eta' K^*$ fits, since the nonresonant $\eta' K\pi$ component is already included in the LASS model.

PDF shapes for the signals and $B\bar{B}$ background are determined from fits to MC samples, while for the $q\bar{q}$ component we use data sidebands, which we obtain excluding the signal region $5.27 < m_{\rm ES} < 5.29$ GeV and $|\Delta E| < 0.075$ GeV. The calibration of $m_{\rm ES}$ and ΔE is checked by means of large data control samples of B

decays to charmed mesons with topology similar to the decays under study [e.g. $B^+ \to \bar{D}^0(K^+\pi^-\pi^0)\pi^+$, $B^+ \to \bar{D}^0(K^+\pi^-\pi^0)\rho^+$].

We use a combination of Gaussian, exponential, and polynomial functions to parametrize most of the PDFs. For the $m_{\rm ES}$ distribution of the $q\bar{q}$ background component, we use a parametrization motivated by phase-space arguments [21]. The following are free to vary in the fit: the signal and $q\bar{q}$ background yields and charge asymmetries $\mathcal{A}_{\rm ch}$, along with the parameters that most strongly influence the shape of the continuum background.

We perform fits to ensembles of simulated experiments in order to evaluate the potential bias Y_0 on the fitted signal yield, which originates from our neglect of the correlations among the variables. Each such experiment has the same number of signal and background candidates as the data; given that correlations among fit variables are negligible for $q\bar{q}$ events, these are generated from the PDFs, while signal and $B\bar{B}$ background events are taken from fully simulated MC samples. In computing the branching fraction $\mathcal{B}$ for each mode, we subtract Y_0 from the fitted signal yield Y and divide by the selection efficiency ε for signal events, the number of B mesons in our sample, and the product of the branching fractions of the intermediate resonances, $\prod \mathcal{B}_i$. We assume the branching fraction of $\Upsilon(4S)$ to B^+B^- and $B^0\bar{B}^0$ to be the same and equal to 50%, consistent with the measurements [14]. The efficiency ε is evaluated from the simulation.

The different submodes of $\eta' K^{*0}$ and $\eta' K^{*+}$ are combined by adding their $-2\ln\mathcal{L}$ curves. For the significance of observation S, we take the difference between the value of $-2\ln\mathcal{L}$ for the zero signal hypothesis and the value at its minimum. For modes with a significance below 5 standard deviations, we quote a 90% confidence level upper limit, corresponding to the branching fraction below which lies 90% of the total of the likelihood integral, in the region where the branching fraction is positive. The correlated and uncorrelated systematic uncertainties are taken into account in the above evaluations by convolving the likelihood function given by the fitter with a Gaussian function

TABLE II. Signal yield Y and its statistical uncertainty, bias Y_0, detection efficiency ϵ, daughter branching fraction product $\prod \mathcal{B}_i$, significance S (with systematic uncertainties included), measured branching fraction $\mathcal{B}$ with statistical and systematic errors, 90% confidence level upper limit, and charge asymmetry $\mathcal{A}_{\rm ch}$. In the case of $\eta' f_0$, the quoted branching fraction is the product of $\mathcal{B}(B^0 \to \eta' f_0)$ with $\mathcal{B}(f_0 \to \pi\pi)$, which is not well known.

Mode	Y (events)	Y_0 (events)	ϵ (%)	$\prod \mathcal{B}_i$ (%)	S (σ)	$\mathcal{B}$ (10^{-6})	$\mathcal{B}$ upper limit (10^{-6})	$\mathcal{A}_{\rm ch}$
$\eta'\rho^0$	37 ± 15	9 ± 5	23.4	17.5	2.0	$1.5 \pm 0.8 \pm 0.3$	2.8	
$\eta' f_0$	8 ± 8	4 ± 2	25.9	17.5	0.5	$0.2^{+0.4}_{-0.3} \pm 0.1$	0.9	
$\eta'\rho^+$	128 ± 22	15 ± 8	14.3	17.5	5.8	$9.7^{+1.9}_{-1.8} \pm 1.1$		$0.26 \pm 0.17 \pm 0.02$
$\eta' K^*(892)^0$					4.0	$3.1^{+0.9}_{-0.8} \pm 0.3$	4.4	$0.02 \pm 0.23 \pm 0.02$
$\eta'_{\eta\pi\pi} K^*(892)^0$	28 ± 10	4 ± 2	18.9	11.7	2.7	$2.4^{+1.1}_{-0.9} \pm 0.3$		-0.04 ± 0.35
$\eta'_{\rho\gamma} K^*(892)^0$	61 ± 18	9 ± 5	13.3	19.6	3.1	$4.3^{+1.6}_{-1.5} \pm 0.5$		0.06 ± 0.29
$\eta' K^*(892)^+$					3.8	$4.8^{+1.6}_{-1.4} \pm 0.8$	7.2	$-0.26 \pm 0.27 \pm 0.02$
$\eta'_{\eta\pi\pi} K^*(892)^+_{K^+\pi^0}$	14 ± 8	2 ± 1	11.5	5.8	2.0	$3.9^{+3.1}_{-2.1} \pm 0.5$		-1.00 ± 0.78
$\eta'_{\rho\gamma} K^*(892)^+_{K^+\pi^0}$	26 ± 19	6 ± 3	9.7	9.8	1.1	$4.7^{+4.5}_{-4.1} \pm 1.3$		0.05 ± 0.66
$\eta'_{\eta\pi\pi} K^*(892)^+_{K^0_S\pi^+}$	23 ± 10	3 ± 2	19.1	4.0	2.6	$5.5^{+2.9}_{-2.4} \pm 0.7$		-0.47 ± 0.37
$\eta'_{\rho\gamma} K^*(892)^+_{K^0_S\pi^+}$	34 ± 15	10 ± 5	16.2	6.8	1.6	$4.8^{+3.2}_{-2.8} \pm 1.2$		0.24 ± 0.44
$\eta'(K\pi)^{*0}_0$					5.6	$7.4^{+1.5}_{-1.4} \pm 0.6$		$-0.19 \pm 0.17 \pm 0.02$
$\eta'_{\eta\pi\pi}(K\pi)^{*0}_0$	106 ± 21	12 ± 6	20.2	11.7	4.9	$8.5^{+2.0}_{-1.9} \pm 1.0$		-0.39 ± 0.20
$\eta'_{\rho\gamma}(K\pi)^{*0}_0$	115 ± 36	21 ± 11	17.6	19.6	2.7	$5.8^{+2.3}_{-2.2} \pm 1.0$		0.32 ± 0.31
$\eta'(K\pi)^{*+}_0$					2.9	$6.0^{+2.2}_{-2.0} \pm 0.9$	9.3	$0.06 \pm 0.20 \pm 0.02$
$\eta'_{\eta\pi\pi}(K^+\pi^0)^{*+}_0$	36 ± 15	2 ± 1	13.9	5.8	2.4	$8.8^{+4.2}_{-3.8} \pm 1.3$		0.00 ± 0.41
$\eta'_{\rho\gamma}(K^+\pi^0)^{*+}_0$	185 ± 51	31 ± 15	12.8	9.8	2.8	$26.4^{+9.0}_{-8.5} \pm 5.9$		0.23 ± 0.27
$\eta'_{\eta\pi\pi}(K^0_S\pi^+)^{*+}_0$	18 ± 12	1 ± 1	18.6	4.0	1.6	$5.1^{+3.5}_{-3.2} \pm 0.9$		0.13 ± 0.59
$\eta'_{\rho\gamma}(K^0_S\pi^+)^{*+}_0$	-29 ± 22	-8 ± 4	17.4	6.8		$-3.8^{+4.0}_{-3.9} \pm 1.5$		-0.40 ± 1.48
$\eta' K^*_2(1430)^0$					5.3	$13.7^{+3.0}_{-2.9} \pm 1.2$		$0.14 \pm 0.18 \pm 0.02$
$\eta'_{\eta\pi\pi} K^*_2(1430)^0$	42 ± 13	2 ± 1	15.1	5.8	3.7	$9.8^{+3.4}_{-3.2} \pm 0.9$		0.58 ± 0.32
$\eta'_{\rho\gamma} K^*_2(1430)^0$	125 ± 26	20 ± 10	10.6	9.8	4.1	$21.7^{+5.4}_{-5.3} \pm 3.0$		-0.05 ± 0.20
$\eta' K^*_2(1430)^+$					7.2	$28.0^{+4.6}_{-4.3} \pm 2.6$		$0.15 \pm 0.13 \pm 0.02$
$\eta'_{\eta\pi\pi} K^*_2(1430)^+_{K^+\pi^0}$	42 ± 11	5 ± 3	9.9	2.9	3.5	$27.1^{+8.8}_{-8.1} \pm 4.5$		0.29 ± 0.25
$\eta'_{\rho\gamma} K^*_2(1430)^+_{K^+\pi^0}$	115 ± 28	20 ± 10	8.5	4.9	2.9	$46.2^{+14.4}_{-13.8} \pm 12.2$		-0.33 ± 0.24
$\eta'_{\eta\pi\pi} K^*_2(1430)^+_{K^0_S\pi^+}$	42 ± 10	5 ± 2	15.3	2.0	4.5	$25.9^{+7.8}_{-7.1} \pm 2.7$		0.44 ± 0.23
$\eta'_{\rho\gamma} K^*_2(1430)^+_{K^0_S\pi^+}$	62 ± 16	14 ± 7	12.4	3.4	3.0	$24.1^{+8.7}_{-8.0} \pm 4.1$		0.22 ± 0.25

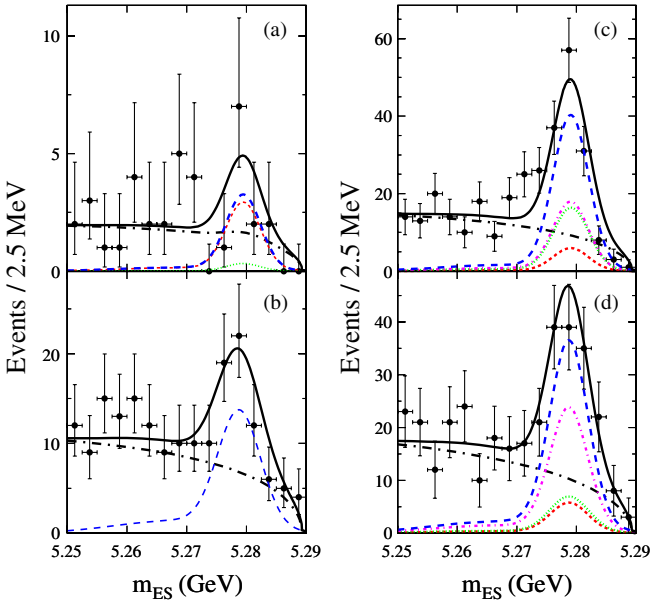

FIG. 1 (color online). *B*-candidate $m_{\rm ES}$ projections for (a) $\eta'\rho^0/\eta' f_0$, (b) $\eta'\rho^+$, (c) $\eta' K^{*0}$, (d) $\eta' K^{*+}$. Color online: the solid curve is the fit function, black long-dash-dotted is the total background, and the blue dashed curve is the total signal contribution. In (a) we separate the ρ^0 component (red dashed) from the f_0 (green dotted). In (c, d) we separate the $K^*(892)$ (red dashed), the $(K\pi)_0^*$ (green dotted), and $K_2^*(1430)$ (magenta dot-dashed) components.

representing the systematic uncertainties. The results are collected in Table II.

We show in Fig. 1 the data and the fit functions projected over the variable $m_{\rm ES}$, while in Fig. 2 we do the same for the $\pi\pi$ and $K\pi$ invariant masses and for $\cos\theta_{\mathcal{H}}$. In these plots the signals are enhanced by the imposition of cuts on $\ln\mathcal{L}$ and the fit variables, which retain 40%–65% of the signal events.

We evaluate the systematic uncertainties due to the modeling of the signal PDFs by varying the relevant parameters by their uncertainty, derived from the consistency of fits to the above mentioned data control samples. The fit bias arises mostly from correlations among the fit variables, which are modeled by the MC; the associated uncertainty is the sum in quadrature of half the correction itself and its statistical uncertainty; this is the dominant source in most cases (2.1–15.4 events), especially for the $\eta' \to \rho^0\gamma$ modes. We verify that the correlations among the variables in SXF events are the major source of bias by performing a dedicated study on simulated experiments in which the SXF component is not embedded. The uncertainty for the SXF fraction is estimated by varying the fraction predicted by the MC by 2.5% (5%) relative for each photon (π^0) in the final state (most of this uncertainty originates from the simulation of neutral particles). We estimate the uncertainty on the charmless $B\bar{B}$ background by repeating the fit with the yield of this component varied by its estimated uncertainty ($\pm$ 20%). For the *S*-wave $K\pi$ components, we

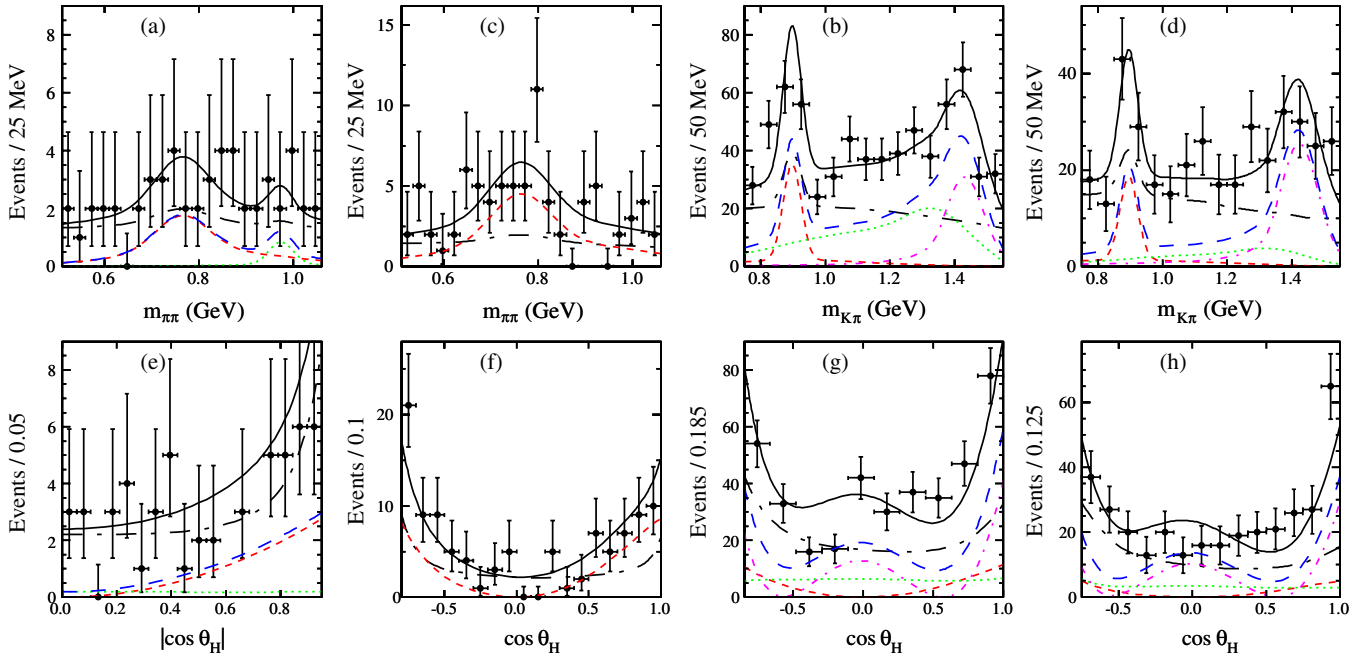

FIG. 2 (color online). Top row: *B*-candidate $m_{\pi\pi}$ projections for (a) $\eta'\rho^0/\eta' f_0$, (b) $\eta'\rho^+$, and $m_{K\pi}$ for (c) $\eta' K^{*0}$, (d) $\eta' K^{*+}$; on the bottom row, we plot the cosine of the helicity angle $\theta_{\mathcal{H}}$ for (e) $\eta'\rho^0/\eta' f_0$, (f) $\eta'\rho^+$, (g) $\eta' K^{*0}$, and (h) $\eta' K^{*+}$. Color online: the solid curve is the fit function, the black long-dash-dotted is the total background, and the blue dashed curve is the total signal contribution. In (a) we separate the ρ^0 component (red dashed) from the f_0 (green dotted). In (c, d) we separate the $K^*(892)$ (red dashed), the $(K\pi)_0^*$ (green dotted), and $K_2^*(1430)$ (magenta dot-dashed) components.

vary the LASS parameters by the uncertainties found in [19] (the resulting uncertainties vary from 0.1 to 14.9 events).

Multiplicative systematic uncertainties (which do not affect the signal significance) account for imperfect knowledge of the luminosity, tracking efficiency, π^0 and K^0_S reconstruction efficiencies, and the uncertainty on the measured branching fractions of intermediate resonances. In the nominal fit we do not account for interference among the different spin K^* components. We estimate in a separate calculation, which takes into account the acceptance functions of our analysis, the potential impact of interference when the relative strong phases between the components are varied over the full range; we find that the uncertainties range from 1.5% to 14.1%.

From the analysis of a variety of data control samples, the bias on $\mathcal{A}_{\rm ch}$ is found to be negligible for pions and -0.01 for kaons, due to differences of K^+ and K^- interactions in the detector material. We correct the fitted $\mathcal{A}_{\rm ch}$ by $+0.01$ in the modes where a charged kaon is present and assign a systematic uncertainty of 0.02, mainly due to the bias correction.

In conclusion, we have measured the branching fraction of B mesons to nine different final states; we claim observation of four of these, while we obtain robust evidence for several others. We compute the branching fraction for $\eta' K^*_0(1430)$ using the composition of $(K\pi)^*_0$ from [20]. We find $\mathcal{B}(B^0 \to \eta' K^*_0(1430)^0) = (6.3 \pm 1.3 \pm 0.5 \pm 0.7) \times 10^{-6}$ and $\mathcal{B}(B^+ \to \eta' K^*_0(1430)^+) = (5.2 \pm 1.9 \pm 0.8 \pm 0.6) \times 10^{-6}$, where the third error comes from the uncertainty in the $K^*_0(1430) \to K\pi$ branching fraction [14]. No significant direct CP violation is seen in the investigated channels. Our results are consistent with and supersede those reported in [7]. Our measured branching fraction for $B^+ \to \eta' \rho^+$ favors the predictions based on pQCD and QCDF over those based on SCET. As in the $B \to \omega K^*$ case, we observe an enhancement of the tensor $K^*_2(1430)$ over the vector $K^*(892)$; this has not been anticipated by the theoretical calculations.

We are grateful for the excellent luminosity and machine conditions provided by our PEP-II colleagues, and for the substantial effort from the computing organizations that support *BABAR*. The collaborating institutions wish to thank SLAC for its support and kind hospitality. This work is supported by DOE and NSF (USA), NSERC (Canada), CEA and CNRS-IN2P3 (France), BMBF and DFG (Germany), INFN (Italy), FOM (The Netherlands), NFR (Norway), MES (Russia), MICIIN (Spain), and STFC (United Kingdom). Individuals have received support from the Marie Curie EIF (European Union), the A. P. Sloan Foundation (USA), the Binational Science Foundation (USA-Israel), and the University of Colorado at Boulder Graduate School.

[1] H.-Y. Cheng and J. G. Smith, Annu. Rev. Nucl. Part. Sci. **59**, 215 (2009).
[2] M. Beneke and M. Neubert, Nucl. Phys. **B651**, 225 (2003).
[3] X. Liu *et al.*, Phys. Rev. D **73**, 074002 (2006); A. G. Akeroyd, C. H. Chen, and C. Q. Geng, Phys. Rev. D **75**, 054003 (2007).
[4] M. Beneke and M. Neubert, Nucl. Phys. **B675**, 333 (2003).
[5] W. Wang, Y. M. Wang, D. S. Yang, and C. D. Lu, Phys. Rev. D **78**, 034011 (2008).
[6] C.-W. Chiang and Y.-F. Zhou, J. High Energy Phys. 03 (2009) 055.
[7] B. Aubert *et al.* (*BABAR* Collaboration), Phys. Rev. Lett. **98**, 051802 (2007).
[8] J. Schümann *et al.* (Belle Collaboration), Phys. Rev. D **75**, 092002 (2007).
[9] X. Liu, Z. Q. Zhang, and Z. J. Xiao, Chin. Phys. C **34**, 157 (2010).
[10] J. H. Munoz and N. Quintero, J. Phys. G **36**, 095004 (2009).
[11] B. Aubert *et al.* (*BABAR* Collaboration), Phys. Rev. D **79**, 052005 (2009).
[12] B. Aubert *et al.* (*BABAR* Collaboration), Nucl. Instrum. Methods Phys. Res., Sect. A **479**, 1 (2002).
[13] The mass and width of the $f_0(980)$ are from the Breit-Wigner parameters obtained by E. M. Aitala *et al.* (E791 Collaboration), Phys. Rev. Lett. **86**, 765 (2001).
[14] C. Amsler *et al.* (Particle Data Group), Phys. Lett. B **667**, 1 (2008).
[15] S. Brandt *et al.*, Phys. Lett. **12**, 57 (1964); E. Farhi, Phys. Rev. Lett. **39**, 1587 (1977).
[16] B. Aubert *et al.* (*BABAR* Collaboration), Phys. Rev. Lett. **99**, 171803 (2007).
[17] K. S. Cranmer, Comput. Phys. Commun. **136**, 198 (2001).
[18] The *BABAR* detector Monte Carlo simulation is based on GEANT4, S. Agostinelli *et al.*, Nucl. Instrum. Methods Phys. Res., Sect. A **506**, 250 (2003); and EvtGen, D. J. Lange, Nucl. Instrum. Methods Phys. Res., Sect. A **462**, 152 (2001).
[19] D. Aston *et al.* (LASS Collaboration), Nucl. Phys. **B296**, 493 (1988).
[20] B. Aubert *et al.* (*BABAR* Collaboration), Phys. Rev. D **72**, 072003 (2005); **74**, 099903(E) (2006).
[21] H. Albrecht *et al.* (ARGUS Collaboration), Phys. Lett. B **241**, 278 (1990).